Journal of The Electrochemical Society, **153** (2) A366-A371 (2006)
0013-4651/2005/153(2)/A366/6/$20.00 © The Electrochemical Society

Toward Improving the Performance of PEM Fuel Cell by Using Mix Metal Electrodes Prepared by Dual IBAD

Andrea F. Gullá,[a,z] Madhu Sudan Saha,[b,*] Robert J. Allen,[a,*] and Sanjeev Mukerjee[b,*]

[a]*E-TEK Division of De Nora North America, Incorporated, Somerset, New Jersey 08873, USA*
[b]*Department of Chemistry and Chemical Biology, Northeastern University, Boston, Massachusetts 02115, USA*

Dual ion beam assisted deposition (IBAD) has been used to manufacture selected Pt-based alloy/mix (Pt–Co and Pt–Cr) electrode-catalysts by direct metallization of a standard E-TEK gas diffusion layer (GDL). Their kinetics for oxygen reduction reaction and their performance in a proton exchange membrane fuel cells (PEMFCs) are presented. Activity enhancement, normalized to electrochemical surface area and mass activity, of 38.99 mA/cm^2 (Pt–Co) and 27.21 mA/cm^2 (Pt–Cr) are reported relative to an IBAD Pt electrode-catalyst. We report a significant new development in terms of materials and mass-manufacturability for PEMFC applications
 [DOI: 10.1149/1.2165571]

Manuscript submitted September 2, 2005; revised manuscript received October 14, 2005.
Available electronically December 30, 2005.

Proton exchange membrane fuel cells (PEMFCs) with their higher efficiency, low heat and noise signature, fuel flexibility, continuous operation, and modularity are an attractive choice over competitors such as batteries and internal combustion engines for portable and stand-alone power generation. As one might realize, the use of Pt-based catalyst represents one of the main limitations to commercial realization of this technology. In the last decade, much of the developmental work has been focused on ways to improve the performance of polymer electrolytes, electrocatalyst, and electrode materials[1,2] while decreasing the amount of precious metal present in the system. The introduction of supported platinum on carbon black has already helped lower the platinum loadings of PEMFCs from several mg$_{Pt}$/cm^2 to about 0.4–0.5 mg$_{Pt}$/cm^2.[3,4] Researchers at Los Alamos National Laboratories[3,4] were able to bring the cathode platinum loading down to 0.12 mg$_{Pt}$/cm^2 with no detrimental effect on fuel cell performance. Concurrently, efforts at Texas A&M University also exhibited great strides toward lowering Pt loading with loadings as low as 0.05 mg$_{Pt}$/cm^2 with comparable performance to those previously reported with 5 mg$_{Pt}$/cm^2.[3,5]

In a recent report on activity benchmarks and future requirements for electrocatalysts in the context of PEM fuel cells, Gasteiger et al.[6] have pointed out that, for automotive application, the current state-of-the-art (with H_2/air at 80°C), approximately 0.7 W/cm^2 at 0.68 V (for 58% energy conversion) corresponding to 0.85–1.1 g$_{Pt}$/kW, still requires further improvement in order to achieve an overall Pt utilization of 0.2 g$_{Pt}$/kW at 0.65 V and above. Achievement of this target can be envisaged as a dual effort wherein (*i*) the membrane electrode assembly (MEA) power density is improved to 0.8–0.9 W/cm$^2_{MEA}$ at 0.65 V and above by increasing Pt utilization and lowering mass transport and ohmic contributions and (*ii*) the inherent activities of the reaction zone is increased by changing the nature of the conventional supported Pt electrocatalysts (Pt nanoparticles) via means such as alloying and modification of surface morphology. In this context it is important to note that the noble metal loading at the anode can be reduced, from the current loadings of 0.2–0.4 mg/cm^2, to about 0.05 mg$_{Pt}$/cm$^2_{MEA}$ without concomitant losses at the anode.[7] Hence the principal effort in this context involves the cathode electrode.

All of this technology has to be tempered with the ability to translate product developments into mass manufacturability while keeping reproducibility (batch vs continuous) as well as cost in perspective. Depending on the deposition methods used, the approach toward lowering noble metal loading can be classified into five broad categories, (*i*) thin film formation with carbon supported electrocatalysts,[8,9] (*ii*) pulse electrodeposition of noble metals (Pt and Pt alloys),[10] (*iii*) sputter deposition,[11] (*iv*) pulse laser deposition,[12] and (*v*) ion-beam deposition.[13] While the principal aim in all these efforts is to improve the charge-transfer efficiency at the interface, it is important to note that while some of these approaches provide for a better interfacial contact allowing for efficient movement of ions, electrons, and dissolved reactants in the reaction zone, others additionally effect modification of the electrocatalysts surface (such as those rendered via sputtering, electrodeposition, or other deposition methods).

Provided below is a concise description of the current state-of-the-art in furthering electrocatalyst utilization, following which is a brief overview of the current understanding of attempts to tweak the electronic and short-range atomic order of Pt for further lowering oxygen reduction reaction (ORR) overpotential. Toward improving the reaction zone, the first of the five broad categories mentioned earlier, using the thin film approach in conjunction with conventional carbon supported electrocatalysts, has several variations which have been reported. These include the so-called decal approach where the electrocatalyst layer is cast on a polytetrafluoroethylene (PTFE) blank and then decaled onto the membrane.[8,9] At its core this approach relies on extending the reaction zone further into the electrode structure away from the membrane, thereby providing for a more three-dimensional zone for charge transfer. Among the limitations of using this approach are problems such as controlling the Pt particle size (with loading on carbon in excess of 40%), uniformity of deposition in large scale production, and most of all cost (due to the complex, several step processes involved).

An alternative method for enabling higher electrocatalyst utilization has been attempted with pulse electrodeposition. Taylor et al.[10] was one of the first to report this approach; pulse electrodeposition was used in conjunction with Pt salt solutions which relied on their diffusion through thin Nafion films on carbon support enabling electrodeposition in regions of ionic and electronic contact on the electrode surface. A recent review on this method also by Taylor et al., describes in detail the technique of pulse electrodeposition of catalytic metals.[14] In principle this methodology is similar to the thin film approach described above; albeit with more efficient electrocatalyst utilization since the catalyst deposition occurs at the most efficient contact zones for ionic and electronic pathways. Though attractive, there are serious concerns on the scalability of this method for mass manufacturing.

Sputter deposition of metals on carbon gas diffusion media is another alternative method which has been widely used. Here, however, the interfacial reaction zone is more in the front surface of the electrode at the interface with the membrane. The original approach in this case was to put a layer of sputter deposit on top of a regular

* Electrochemical Society Active Member.
z E-mail: a.gulla@etek-inc.com

Pt/C containing a conventional gas diffusion electrode (GDE). Such an approach[15] exhibited a boost in performance by moving part of the interfacial reaction zone in the immediate vicinity of the membrane. Recently, Hirano et al.[11] reported promising results with a thin layer of sputter-deposited Pt on wet proofed noncatalyzed gas diffusion layer (equivalent to 0.01 mg_{Pt}/cm^2) as compared to a commercially available Pt/C (0.4 mg_{Pt}/cm^2) electrode. In most cases the deposition has relatively poor adherence to the substrate and under variable conditions of load and temperature, there is a greater probability of dissolution and sintering of the deposits.

An alternative method providing for direct deposition, recently reported, uses pulsed laser deposition.[12] Excellent performance was reported with loading of 0.017 mg_{Pt}/cm^2 in a PEMFC, however the electrodes prepared were only tested as anodes, no cathode application has been reported to date.

In all the above methodologies presented, mass manufacturability with adequate control on reproducibility remains questionable at best. In this regard the methodologies developed by the 3M Company are noteworthy, where mass manufacture of electrodes with low noble metal loading is reported.[16,17] Here a series of vacuum deposition steps are involved with adequate selection of solvents and carbon blacks resulting in nanostructured noble-metal-containing carbon fibrils which are embedded into the ionomer-membrane interface.[18,19]

In conventional catalyst-chemistry, one of the most elegant approaches in trying to lower the cost of a pure Pt electrode-catalyst is by alloying platinum with other less expensive transition metals. From a systems standpoint, the primary technical challenge common to both reformer-based and direct methanol low and medium temperature PEMFCs is the large overpotential loss as well as the generally poor kinetics of the ORR. The relatively high overpotential losses ($\sim$220 mV) in the low current density region of the ORR[20,21] with the current state-of-the-art low Pt loading electrodes (0.1 to 0.2 mg/cm^2) is a result of a mixed potential at the oxygen electrode due to a combination of slow O_2-reduction kinetics and competing anodic process such as Pt-oxide formation and/or impurity oxidation.[22] Many Pt-based transition metal alloys have been suggested for use as a PEMFC cathode catalyst[23-25] with varying degrees of enhancement as compared to Pt. Changes in short-range atomic order, particle size, Pt d-band vacancy, Pt skin effects, and Pt-OH inhibition have been proposed as the responsible factors for the enhanced performance of these alloys[26-29] (see Adzic[30] and Mukerjee[31]). As reported recently, from a mechanistic standpoint, Pt-based alloys have the tendency to inhibit or shift the onset potential (approximately 800 mV vs RHE for Pt) of Pt–OH formation, thus providing free sites for molecular oxygen adsorption.[32] The immediate consequence of such behavior is represented by the lowering of the overpotential losses; evidence of this improvement has been reported in earlier work.[23,33,34] Shifting the onset potential of OH formation on Pt is dependent on (*i*) the ability of the alloying elements to modify the Pt electronic and short-range atomic order for inhibiting activation of H_2O and (*ii*) the ability of the alloying element to attract and hold H_2O_{ads} more strongly than the surrounding surface Pt atoms.[35]

Recently, the use of ion-beam techniques has been reported, where the benefits of low energy ion bombardment concurrent with thin film vacuum deposition (electron beam) process is exploited for achieving dense, adhering, and robust depositions.[36] In recent publications from our group,[37] we have shown that with Pt it is possible to get a mass specific power density of 0.3 g_{Pt}/kW (at 0.65 V) with a 250 Å layer using a dual ion beam deposition process, this corresponded to a total MEA loading of 0.08 mg/cm^2.[37,38] This was in contrast to conventional Pt/C-based MEAs with typical specific power density of 1.2 g_{Pt}/kW (at 0.65 V) corresponding to 1 gm/cm^2 MEA loading.[38,39]

The objective of this work is to present an improved deposition methodology based on an ion deposition technique in conjunction with use of a bimetallic-layered structure to provide an alternative ultralow loading Pt-based electrode which is amenable to mass production with low cost, and high reproducibility. This is important from the perspective of conventional methods of Pt-binary and ternary transition-metal-supported electrocatalyst preparation, where reproducibility and cost are matters of grave concern. The goal is therefore to overcome many of the limitations previously mentioned and to produce a Pt electrode having (*i*) better electrocatalyst utilization of the precious metal, (*ii*) very low precious metal (Pt) loading, and (*iii*) provide for a more enhanced electroactive surface for ORR with the use of bimetallic deposits. The electrodes prepared were comprised of two layers (each one 500 Å thick); the first layer was either Co or Cr while the second layer was pure metal Pt. The mix metal electrodes prepared by the ion beam assisted deposition (IBAD) technique are tested in PMEFC to investigate their oxygen reduction reaction activity and single-cell performance. In addition, the electrodes were characterized by X-ray diffraction (XRD), scanning electron microscopy (SEM) and electrochemical measurement.

Experimental

Electrode preparation.— Dual IBAD is a vacuum-deposition process that combines physical vapor deposition (PVD) with ion-beam bombardment. Vapors of coating atoms are generated with an electron-beam evaporator and deposited on a substrate. Ions are simultaneously extracted from the plasma and accelerated into the growing PVD film at energies of several hundred to several thousand electron volts (500 to 2000 eV). Ion bombardment is the key factor controlling film properties in the IBAD process; thus imparting substantial energy to the coating and coating/substrate interface. This achieves the benefits of substrate heating (which generally provides a denser, more uniform film) without degrading its bulk properties. The major parameters of the process are coating material, evaporation rate, ion species, ion energy, and ion-beam and current density; the influence of all these parameters are described in detail elsewhere.[39-41] In this work, dual-IBAD was used to directly deposit two distinct metal layers onto a commercially available noncatalyzed GDL (LT1400-W, E-TEK). The first one (directly on top of the GDL) was comprised of either Co or Cr metals while the second one (deposited directly on top of the first metal layer) was comprised of pure Pt. All layers deposited had a prechosen thicknesses of 500 Å thus giving a total precious metal loading of about 0.08 mg/cm^2. The thicknesses of all the electrodes prepared were measured by analyzing a reference Si wafer coupon which was strategically located with the roll of carbon cloth during the deposition process. A profilometer was used to measure the thickness of the deposit on the Si wafer. This served as a direct correlation of deposition thickness on the GDL. The loadings were additionally measured by analyzing a statistically significant number of samples of known geometric area with the aid of the standard thermogravimetric analysis method. This allowed for a sensitive measurement of the effective loading of each sample, found to be within a 10% margin of error. Finally, the GDL used as the substrate consisted of a three-dimensional woven web structure comprised of a carbon cloth support as a substrate with a coating of wet-proofed carbon. From a structural standpoint, the GDL (LT1400-W, E-TEK) used possessed improved tensile properties and surface roughness[42] which is perfectly suited for such superficial metal deposition obtained through IBAD.

Preparation of the membrane and electrode assembly.— The MEA were prepared using a Nafion 112 membrane (DuPont); prior to MEA fabrication the membrane was cleaned by immersion in boiling 3% H_2O_2 for 1 h followed by boiling 1 M H_2SO_4 for the same duration with subsequent rinsing in boiling deionized water (1 h). The last step in this procedure was repeated at least twice to ensure complete removal of H_2SO_4. The MEA was fabricated in-house via hot pressing ($100°C < T < 130°C$, $5\ min < t < 10\ min$, and $200\ psig < P < 400\ psig$). Contrary to the conventional MEA assemblies, no extra liquid ionomer was used in the MEA fabrication.

Assembly of the single cell and its installation in the test station.— All MEAs were tested in a 5 cm^2 single-cell fuel cell (Fuel Cell Technologies, Albuquerque, NM) using a standard fuel cell test station (built in-house) designed to carry out steady-state polarization measurements. This cell allowed for simultaneous measurements of both single- and half cell data with the aid of reference electrodes in the anode chamber (hydrogen reference). The fuel cell test station also allowed for independent control of humidification, cell temperature, and gas flow rate. All MEAs were conditioned prior to testing using a series of steps; the initial step involved a so-called break-in process in which the cell temperature was slowly raised (approximately 20°C/h) from ambient temperature to the operational temperature under N_2. After keeping the cell under these conditions for approximately 5 h in order to enable proper conditioning of the MEA assembly, the pressure was slowly increased to 50/60 psig (anode/cathode, respectively). The gases were then switched to saturated H_2 and air/O_2 and the cell was allowed to equilibrate for a couple of hours.

Cyclic voltammetry was conducted at room temperature using an Autolab potentiostat/galvanostat (model, PGSTAT-30, Ecochemie, Brinkman Instruments). The electrodes, in a completely flooded configuration were cycled both in the presence and absence of CO in 1 M $HClO_4$. For CO stripping voltammetry, pure CO was purged close to the working electrode for at least 1 h with the electrode polarized at 0.05 V vs RHE in a fume hood. The electrode was then purged with pure N_2 for 1 h followed by voltammetric stripping. All cyclic voltammetric experiments were recorded between 0.05 and 1.2 V with a scan rate of 20 mV/s.

The morphological characterization of the electrodes was conducted using SEM energy dispersive X-ray analysis (EDAX) technique (Hitachi field emission SEM/EDAX, model no. 5800 with Genesis model 136-10 EDAX containing a Z-max window for lighter elements). The SEM image was observed at different points along the electrode top surface and lateral cross-section. For the lateral cross-section a microtome (Reidhert ultracut model no. E with a diamond knife) with 0.5 μm section size was used. The EDAX was conducted simultaneously. The EDX spectrum was recorded at several points along the cross section by moving the sample under the electron gun, using an *x-y* manipulator.

Results and Discussion

To aid the reader in the understanding of the nomenclature used to identify the samples studied, we adopt the terminology GDL diffuser (LT1400-W, E-TEK) as having no metal deposition or catalyst. The term IBAD500 Pt refers to an electrode that was prepared by deposition of a 500 Å layer of solely pure Pt metal while the term IBAD Pt–Co and IBAD Pt–Cr refer to the electrodes prepared by depositing the bilayer metals (in which the deposition is of 500 Å, initially with the transition metal followed by a further 500 Å for Pt layer).

Morphological aspects.— The XRD patterns for the bilayered IBAD GDEs and a standard IBAD500 GDE (Pt based) are shown in Fig. 1. The diffraction lines are superimposed on the background represented by the noncatalyzed GDL, the powder diffraction for Pt/C (E-TEK) is also shown for comparison. In addition, the internal sample reference (Al, showing the characteristic five sharp peaks) was used to align the various diffraction patterns. Judging from the spectroscopic features represented by (111) diffraction peak ($2\Theta = 39.764°$) and using the peak width at half intensity (Scherrer treatment), the crystallite size of the diffracting domains range between 90 and 100 Å (or 9.0/10 nm). This is larger than those typically obtained for the conventional Pt/C electrocatalysts (as shown in Fig. 1), where the typical size of diffracting domains are in the range of 2–4 nm.[43] Further, in contrast with supported PtM/C, which under conditions of proper alloy formation exhibits expected line shifts in XRD profiles corresponding to a decrease in lattice parameters,[43] IBAD represents a bilayered coating of M (either Co or Cr) followed by Pt metal deposition. The relatively thin and correspondingly lower density deposits are therefore largely amorphous. As a result only the principal diffraction line (111) is visible for Pt, evidence of transition metals in the diffraction pattern for bimetallic deposits is totally absent representing the complete amorphous nature of the deposit. Further no shift was detected in any of the Pt's diffracting line positions (2Θ shift of the main (111) diffraction line) for the Pt–Co and Pt–Cr IBAD samples, thus indicating the absence of an intermetallic Pt-M alloy formation. While no evidence of alloy formation was observed through conventional X-ray measurements, it is possible to envision the presence of a very thin layer of intermetallic alloy, located at the interface between the two metals (Pt-M).

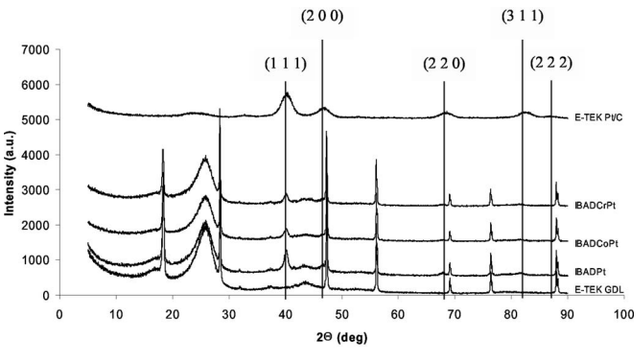

Figure 1. XRD patterns of the IBAD electrodes (Pt IBAD500, IBAD Pt–Co, and IBAD Pt–Cr), corresponding pattern for a Pt/C (E-TEK) electrocatalyst (40% Pt on C) and uncatalyzed E-TEK-GDL (LT1400) are also shown. The 2θ angles are in reference to a Cu Kα source corresponding to a wavelength of (λ = 1.54 Å). The principal diffraction lines for Pt are marked in the figure. Note the lack of secondary diffraction lines for the IBAD deposits, showing the amorphous nature of the deposits. Also missing are any diffraction lines for the codeposited transition metals Co and Cr.

Figure 2 shows the SEM micrographs taken for noncatalyzed GDL (Fig. 2a) and after metallization, the Pt IBAD500 GDE (Fig. 2b) with a magnification of 50,000 times. As evident from the comparison, the top surface of the gas diffusion layer is uniformly coated by the Pt deposited layer. Also, no change in the surface morphology of the carbon support is observed, i.e., the intrinsic porous structure of the gas diffusion layer remains practically unchanged after metallization. This is very important from the perspective of mass transport of dissolved reactants to the IBAD deposits (reaction centers) and the removal of water at the cathode electrode. Figure 2c and d show the representative cross-sectional view of the IBAD Pt–Co GDE with a magnification of about 50,000 times; here the layered metal deposition is visible as localized at the top surface of the noncatalyzed GDL. A deeper analysis from the prospective of the electrode cross section shows the layered nature of the metal deposition as evident from the fluorescence signal of Co and Pt (EDAX analysis) in Fig. 2d which shows two distinctive metal layers with the first one being the transition metal of choice (Co in this particular case) and the second one, or outer most, being pure Pt. Further analysis of this cross section using EDAX will be presented in a full version of this paper. In summary, as observed from Fig. 2, the IBAD deposition strictly results in a very well-defined gas diffusion electrode structure; thus creating an interface region that greatly differs from the conventional MEA design. In the latter case the motivation is to extend the electrochemical polymer electrolyte-electrode interface further into the electrode reaction layer. In the IBAD-type electrode, the interface is pushed further toward the immediate interfacial zone with the polymer electrolyte membrane. In addition the relative thick metallization layer has an intrinsic porosity bearing the same signature porosity as the underlying GDL.

Electrochemically active surface area and catalyst utilization.— The cyclic voltammograms for the IBAD electrodes is shown in Fig. 3. In this case both the hydrogen adsorption/

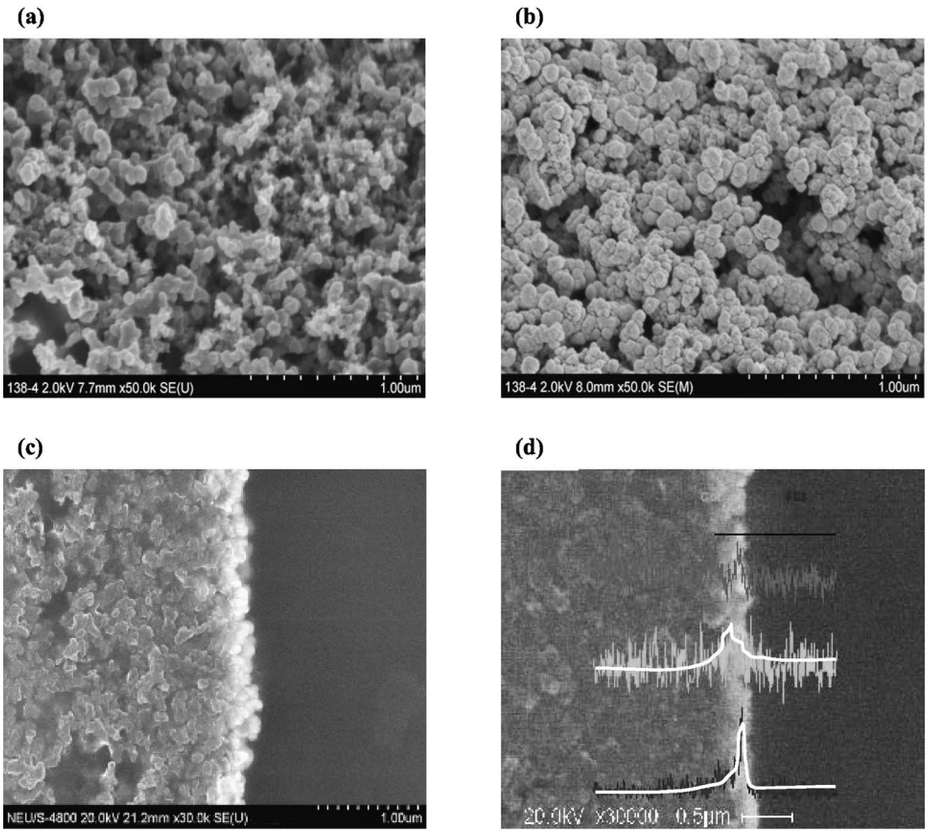

Figure 2. SEM micrograph of (a) uncatalyzed GDL (LT1400, E-TEK) compared to (b) corresponding micrograph for IBAD 500 Pt. Cross-sectional SEM of the Pt IBAD500 is shown in (c), the corresponding crosssection of the Co–Pt IBAD is shown in (d) along with the associated EDAX profiles showing C-K, Co-L, and Pt-M lines in the fluorescence signal.

desorption areas as well as those from stripping voltammetry of adsorbed CO (CO_{ads}) was used. The objective was to get a proper perspective of the nature of the reactive surface from the point of view of the presence of Pt and surface transition metal oxides. For the roughness factors obtained from H_{ads}/H_{des} peaks (average value), 210 $\mu C/cm^2$ was used for the oxidation of atomic hydrogen, a typical value based on the smooth Pt surface. For corresponding values from CO stripping voltammograms, 420 $\mu C/cm^2$ was used. The CO stripping voltammograms were measured after adsorption of CO on the catalyst surface at 0.05 V vs RHE followed by a N_2 purge (both for 1 h) and the oxidation of the CO_{ads} to CO_2 in a subsequent positive potential scan under flowing N_2. Figure 3 shows CO_{ads} stripping scans for the IBAD Pt–Co and Pt–Cr GDEs, an IBAD750 Pt GDE is shown for comparison. All cyclic voltammograms (CVs) were conducted in a flooded electrode mode (1 M $HClO_4$). The roughness factor (r_f) and the real Pt surface (A_{Pt},m^2/g_{Pt}) from CO_{ads} stripping were measured using the following equations

$$r_f(cm^2/cm^2) = Q_{COads}/420\mu C\ cm^{-2}$$

$$A_{Pt}(m^2 g_{Pt}^{-1}) = r_f/\text{Pt loading}$$

The calculated values of roughness factors as well as roughness factors normalized on the basis of Pt loading (cathode electrode) are listed in Table I. CO electrode oxidation potential is strictly governed by the availability of surface oxides according to the following reaction

$$Pt - CO + Pt - OH(\text{or } M - OH) \rightarrow CO_2 + H^+ + (2)Pt(+ M) + e^-$$

The ignition potential of the CO electrode oxidation as well as the stripping peak potential gives a basis of comparison of the CO tolerance of catalysts. The comparison of the CO_{ads} stripping peaks (Fig. 3a) shows distinct differences between the Pt IBAD750 and the Pt–Co and Pt–Cr IBAD GDEs, a shift in the onset of CO_{ads} stripping to the extent of about 45 mV is observed. However, the exact nature of this shift is not completely understood as there are a number of factors at play. Prime parameters are the lower density of the Pt deposits, as well as morphology of the surface deposit (which is very different from conventional supported nanoparticles) and finally the potential presence of surface oxides which form at lower potentials on the non-noble transition metals. It is interesting to note, however, that the H_{ads}/H_{des} peaks exhibited no significant differences (Fig. 3b).

Steady-state polarization behavior in PEMFCs.— Figure 4a shows the cell potential-current density curves (without *iR* correction) at 80°C, 50/60 psig backpressure for anode and cathode electrodes, respectively (100% humidification condition) with H_2/O_2. It is observed that the IBAD Co–Pt GDE shows better performance than Pt IBAD500 GDE especially in the low current density activation-controlled region. For the MEA made with IBAD Co–Pt GDE, the fuel cell performance at 0.8 V is 0.24 and 0.48 A/cm^2 in H_2/air and H_2/O_2, respectively, with a total Pt loading of 0.16 mg_{Pt}/cm^2 per MEA (0.08/0.08 mg_{Pt}/cm^2 anode/cathode loadings), the resulting power densities are ca. 0.20 and 0.38 W/cm^2 (at 0.8 V). This relatively higher performance of the cell (compared to Pt IBAD500 GDE) does not seem to be significantly attributable to the electrochemically active surface area of the electrode (Table I). One of the yardsticks for the potential use of PEMFCs for automotive use, as pointed out recently by Gasteiger et al.[6] is the need to transition from the current state of the art, 0.7 W/cm^2 (at 0.65 V, conversion efficiency 55%) corresponding to a Pt-specific power density of 0.85–1.1 g_{Pt}/kW to less than 0.2 g_{Pt}/kW at 0.65 V and above (55% energy conversion), translating to a target of area-specific power density in the range of 0.8 to 0.9 W/cm^2_{MEA} at 0.65 V and above. The current state of the art is close to perfor-

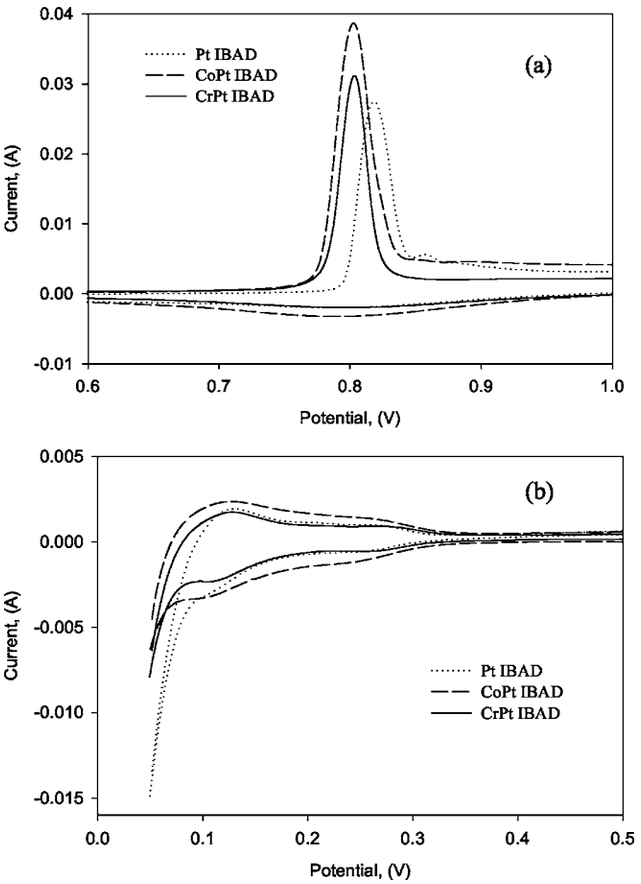

Figure 3. Cyclic voltammograms for IBAD electrodes (a) with CO and (b) without CO at 25°C, corresponding to a scan rate: 20 mV/s. All measurements were made at room temperature in the standard 5 cm^2 PEM single cell under fully humidified conditions. Note the negative shift in the onset of CO stripping for the Co–Pt and Cr–Pt IBAD electrodes, indicative of the effect of surface oxides corresponding to these non-noble transition metals.

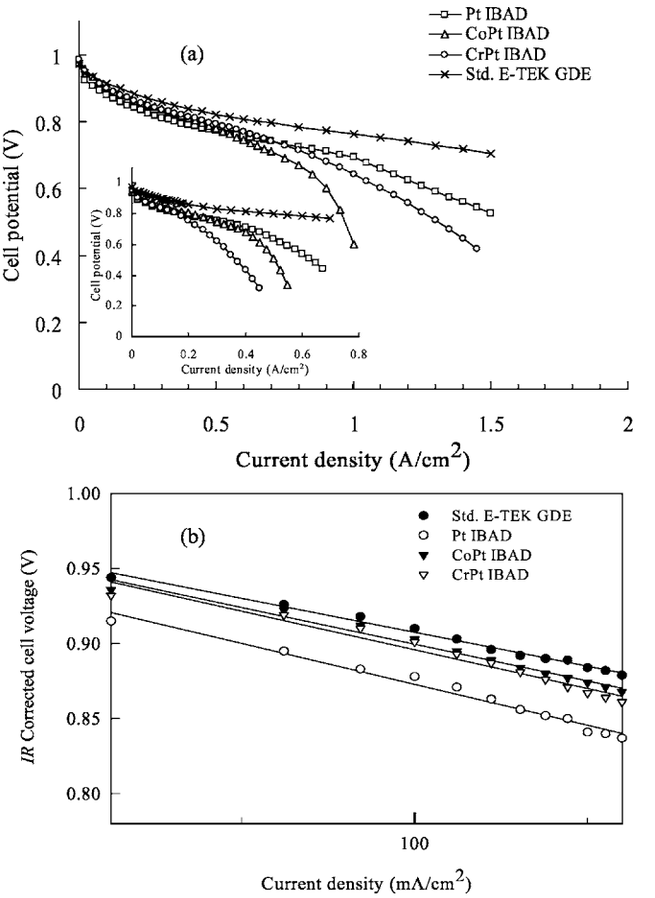

Figure 4. (a) Steady-state polarization measurements in 5 cm^2 PEMFC single cell set up with H_2/O_2 and (b) *iR*-free Tafel plots for oxygen reduction. The cell operating conditions were 80°C, 50/60 psig anode and cathode back pressure, Nafion 112 membrane. Inset shows steady-state polarization with H_2/air.

mance with H_2/air at 80°C (full humidification) using Pt/C commercial electrodes from E-TEK obtained in this investigation (Fig. 4a).

Under conditions of H_2/air feed at 80°C, the MEA prepared with Pt IBAD500 GDE (0.16 $mg_{Pt(MEA)}/cm^2$) resulted in a power density of 0.327 W/cm^2 at 0.65 V, translating into a Pt-specific power density of 0.734 g_{Pt}/kW. Hence while the area specific power density is lower, the gravimetric power density is an improvement. The lower area specific power density for Pt IBAD500 GDE as compared to E-TEK GDE, as well as the Pt-M IBAD GDEs, is due to the higher mass-transport induced voltage losses for the former case. It is therefore clear that further improvement of the GDL substrate is required in the case of the IBAD electrodes.

As has been carried out previously,[44] the data up to the end of the linear region of the half-cell potential (E) vs current density (i), were analyzed using the following equation

$$E = E_o - b \log i - Ri \quad [1]$$

where

$$E_o = E_r + b \log i_o \quad [2]$$

E_r is the reversible potential for the electrode, b is the Tafel slope, i_o is the exchange current density for the oxygen reduction reaction (ORR), and R is predominantly the ohmic resistance in the electrode and electrolyte responsible for the linear variation of potential vs current density plot. The parameters E_o, b, and R were evaluated by a nonlinear least square fitting of Eq. 1 to the experimental data. Using the R values, the *iR*-corrected Tafel plots [$(E + iR$ vs $\log i)$] were constructed (Fig. 4b). The *iR*-corrected Tafel plots presented in Fig. 4b shows that a lowering of Pt loading from 0.5 mg_{Pt}/cm^2, of the E-TEK standard GDE, to 0.08 mg_{Pt}/cm^2, in the Pt IBAD500 electrode, results in a loss of *iR*-corrected potential of ~35–40 mV.

Table I. Electrode kinetic parameters for oxygen reduction.

Electrode	E_o (mV)	b (mV/decade)	$I_{900\ mV}$ (mA/cm^2)	$I_{900\ mV}$ (mA/mg Pt)	S_{EL} (cm^2/cm^2)	$A_{Pt,MEA(ca)}$ ($m^2\ g_{cat}^{-1}$)
IBAD500 Pt	1009	68.5	59.82	747.84	20.31	25.39
IBAD CoPt	1023	61.4	98.81	1235.23	29.46	36.83
IBAD CrPt	1026	64.6	87.03	1087.81	21.21	26.51

Assuming no increase in the mass-transport losses, the change in cell voltage as a function of cathode Pt loading can be described mathematically on the basis of the known O_2 reduction kinetics[45]

$$\left.\frac{\delta E}{\delta \log[L_{ca}]}\right|_{P_{O_2},P_{H_2}T,i} = -b \qquad [3]$$

where L_{ca} denotes the cathode Pt-loading. Equation 3 states that the change in cell voltage with the logarithm of the cathode Pt-loading (assuming the same catalyst is used) is proportional to the Tafel-slope. For a Tafel-slope of 60–70 mV/decade at 80°C, a loading reduction by a factor of 2 or 4 is predicted to lead to a voltage loss across the entire current density range of ≈20 or ≈40 mV, respectively. This assumption can be expected to hold till the end of the ohmic controlled region, i.e., 200 mA/cm^2. Further a comparison with the E-TEK Pt/C GDE (albeit a different morphology) indicates that the difference in overpotential of ~35–40 mV is an expected result, considering the difference in loading which is greater than sixfolds. When the *iR*-corrected potentials of the standard E-TEK Pt electrode-catalyst (0.5 mg$_{Pt}$/cm^2) and Pt-M IBAD electrodes (0.08 mg$_{Pt}$/cm^2) are also compared, the true enhanced nature of these surfaces becomes clearly evident. As presented in Fig. 4b, the activation overpotential difference between the Pt-M IBAD GDEs and the standard E-TEK GDE is only of ~5 to 10 mV. This behavior resembles the one of a conventional Pt-based alloy electrode catalyst. Nevertheless, the lower overpotential loss of the Pt-M IBAD GDEs, represents an even more tangible improvement on the standard Pt IBAD500 GDE.

The nonalloyed character of the Pt-M IBAD deposition opens a fundamental question regarding the true nature and characteristics required in the design of a true Pt-based alloy catalyst. Issues such as durability, overall performance, catalytic efficiency, ease of production, and, most of all, comparison with conventional Pt-based alloy electrode-catalysts will be the focus of a future detailed report.

Conclusions

Dual ion beam-assisted deposition was successfully used to prepare layered metal electrodes for PEMFCs. The first layer was either Co or Cr while the second layer was pure Pt. The morphology of the deposits is very different from those typically encountered in carbon-supported Pt electrocatalysts, both from the perspective of the relative population of the surface crystalline planes as well as particle-size distribution. When compared to the standard IBAD prepared electrodes, the overall fuel cell performance was increased thus mimicking the same effect observable when a carbon-supported alloy is prepared according to conventional means. The dual IBAD approach, as shown in this investigation, is one in which two ion beams were used; one to roughen the substrate and the other to embed the target atoms (Pt, Co, and Cr). Some differences were observed in the onset potential of CO_{ads} stripping which could be correlated with changes in the crystalline nature of the deposit as well as the presence of non-noble metal oxides, and future tests will focus more on the tolerance to Co of the IBAD-prepared electrodes. In this regard, also the effect of CO_{ads} stripping and its possible correlation with onset of potential of water activation needs further investigation. Of greater importance, however, is the fact that we obtained enhanced ORR activity with no apparent evidence of alloying. Future efforts also include a careful evaluation of durability of these deposits as compared with the conventional PtM/C electrodes. Overall, this constitutes a major advancement in the mass manufacturability of PEM fuel cell electrodes.

Acknowledgments

This work has been sponsored in part by Department of Energy grant DE-FC04-02AL67606, and it is registered with the Office of Patents and Trademarks under the following numbers: 6,077,621; 6,673,127; 6,017,650; and 6,103,077. The authors gratefully acknowledge the financial support from the Army Research Office (Single Investigator Grant) for the underlying fundamental understanding of the oxygen reduction reaction at PEM interfaces. The authors gratefully thank Dr. Nazih Hakim for his collaboration during the collection of the SEM micrographs, Dr. Enrico Ramunni (De Nora Tecnologie Elettrochimiche S.r.l., Milano, Italy) and Dr. Emory S. De Castro (E-TEK Division of De Nora North America, Inc., Somerset, NJ) for their constructive observations during various phases of the project.

E-TEK Division of De Nora North America assisted in meeting the publication costs of this article.

References

1. K. Kordesch and G. Simader, *Fuel Cells and Their Applications*, p. 73, VCH, Germany (1996).
2. K. B. Prater, *J. Power Sources*, **51**, 129 (1994).
3. S. Srinivasan, E. A. Ticianelli, C. R. Derouin, and A. Redondo, *J. Power Sources*, **22**, 359 (1988).
4. S. Srinivasan, in *Electrode Kinetic and Electrocatalytic Aspects of Electrochemical Energy Conversion*, New York (1992).
5. A. C. Ferreira and S. Srinivasan, in *Electrode Materials and Processes for Energy Storage and Conversion*, S. Srinivasan, D. D. Macdonald, and A. C. Khandkar, Editors, PV 94-23, p. 173, The Electrochemical Society Proceedings Series, Pennington, NJ (1994).
6. H. A. Gasteiger, *Appl. Catal., B*, **56**, 9 (2005).
7. N. M. Markovic, in *Handbook of Fuel Cells-Fundamentals, Technology and Applications*, Vol. 3, W. Vielstich, H. Gasteiger, and A. Lamm, Editors, p. 368, Wiley, Chichester, UK (2003).
8. M. S. Wilson and S. Gottesfeld, *J. Appl. Electrochem.*, **22**, 1 (1992).
9. Y. G. Chun, *J. Power Sources*, **71**, 174 (1998).
10. E. J. Taylor, E. B. Anderson, and N. R. K. Vilambi, *J. Electrochem. Soc.*, **139**, L45 (1992).
11. S. Hirano, J. Kim, and S. Srinivasan, *Electrochim. Acta*, **42**, 1587 (1997).
12. N. Cunningham, E. Irissou, M. Lefevre, M.-C. Denis, D. Guay, and J. P. Dodelet, *Electrochem. Solid-State Lett.*, **6**, A125 (2003).
13. A. F. Gullá, M. S. Saha, R. J. Allen, and S. Mukerjee, *Electrochem. Solid-State Lett.*, **8**, A504 (2005).
14. E. J. Taylor and M. E. Inman (Faraday Technology, Inc., USA), WO Pat. p. 41 (2000).
15. S. Mukerjee, S. Srinivasan, and A. J. Appleby, *Electrochim. Acta*, **38**, 1661 (1993).
16. M. K. Debe, T. N. Pham, and A. J. Steinbach, U.S. Pat. 97,948,857 (1999).
17. M. K. Debe, J. M. Larson, W. V. Balsimo, A. J. Steinbach, and R. J. Zeigler, U.S. Pat. 97,948,627 (1999).
18. M. K. Debe, R. J. Poirer, M. K. Wakerfuss, and R. J. Zeigler, U.S. Pat. 97,948,599 (1999).
19. M. K. Debe, G. M. Haugen, A. J. Steinbach, J. H. Thomas, and R. J. Ziegler, U.S. Pat. 5,879,827 (1999).
20. S. Srinivasan, *J. Electrochem. Soc.*, **136**, 41C (1989).
21. A. J. Appleby and F. R. Foulkes, *Fuel Cells Handbook*, van Nostrand Reinhold, New York (1989).
22. H. Wroblowa, *Chem. Interfacial Electrochem.*, **15**, 139 (1967).
23. J. McBreen and S. Mukerjee, *J. Electrochem. Soc.*, **142**, 3399 (1995).
24. S. Mukerjee, S. Srinivasan, and M. P. Soriaga, *J. Electrochem. Soc.*, **142**, 1409 (1996).
25. S. Mukerjee, S. Srinivasan, and J. A. Appleby, *Electrochim. Acta*, **38**, 1661 (1993).
26. V. Jalan and E. J. Taylor, *J. Electrochem. Soc.*, **130**, 2299 (1983).
27. M. T. Paffet, *J. Electroanal. Chem. Interfacial Electrochem.*, **220**, 269 (1987).
28. K. Kinoshita, *J. Electrochem. Soc.*, **137**, 845 (1990).
29. B. C. Beard and P. N. Ross, *J. Electrochem. Soc.*, **130**, 3368 (1990).
30. R. R. Adzic, in *Electrocatalysis*, J. Lipkowski and P. N. Ross, Editors, p. 197, Wiley-VCH, New York (1998).
31. S. Mukerjee, *J. Appl. Electrochem.*, **20**, 537 (1990).
32. V. S. Murthi, R. C. Urian, and S. Mukerjee, *J. Phys. Chem. B*, **108**, 11011 (2004).
33. S. Mukerjee and S. Srinivasan, *J. Electrochem. Soc.*, **142**, 1409 (1995).
34. S. Mukerjee, *J. Phys. Chem.*, **99**, 4577 (1995).
35. M. Teliska et al., *J. Electrochem. Soc.*, 152, In press.
36. J. K. Hirvonen, *Mater. Res. Soc. Symp. Proc.*, **792**, 647 (2004).
37. A. F. Gulla, M. S. Saha, R. J. Allen, and S. Mukerjee, *Electrochem. Solid-State Lett.*, **8**, A504 (2005).
38. M. S. Saha, *Electrochim. Acta*, In press.
39. R. J. Allen and J. R. Giallombardo. 2000: U.S. Pat.
40. C. A. Cavalca, J. H. Arps, and M. Murthy. 2001: U.S. Pat.
41. M. G. Fernandes, D. A. Thompson, W. W. Smeltzer, and A. Davies, *J. Mater. Res.*, **5**, 98 (1995).
42. http://www.etek-inc.com/standard/product_GDL%20LT.php?prodid=52
43. S. Mukerjee, in *Catalysis and Electrocatalysis at Nanoparticle Surfaces*, A. Wieckowski, E. R. Savinova, and C. G. Vavenas, Editors, Marcel Dekker, New York (2003).
44. E. A. Ticianelli, C. R. Derouin, A. Redondo, and S. Srinivasan, *J. Electrochem. Soc.*, **135**, 2209 (1988).
45. H. A. Gasteiger, J. S. Panels, and S. G. Yan, *J. Power Sources*, **127**, 162 (2004).